Evaluation of precipitation over the Middle East and Mediterranean in high resolution climate models

University of Reading

Department of Mathematics, Meteorology and Physics

David MacLeod

August 2009

Supervisors: Dr. Len Shaffrey and Dr. Emily Black

Submitted in partial fulfilment of the requirements for the degree of
MSc in Mathematical and Numerical Modelling of the Atmosphere and Oceans

Abstract

The Middle East is considered the worlds most water scarce region (Brown & Crawford (2009)). In this study two high resolution climate models have been evaluated to compare how successfully they model precipitation over the region. One model is HiGEM (Shaffrey et al. (2009)), a global coupled ocean-atmosphere model which operates at a resolution of 1.25° x 0.83° in longitude and latitude for the atmosphere, and 1/3° x 1/3° in the ocean. The other model is an atmosphre only regional model operating at a resolution of 0.44° x 0.44° (Black (2009)).

It has been found that both models capture well the seasonal cycle of precipitation well, although the regional model underestimates the total amount. 10m surface wind fields and mean sea level pressure climatologies from the models also have been compared with ERA-40 reanalysis data to investigate the climatic processes represented in the models. It has been found that the Cyprus low is not represented well in the regional model. The Cyprus low is associated with eastward moving weather systems bringing most precipitation to the region - an underestimation of the intensity in the regional model is likely associated with underestimation of precipitation. It has also been found that the regional model underestimates low level convergence in the main region of precipitation and HiGEM overestimates it - likely to be associated with the underestimation and slight overestimation of precipitation in this region in each of the models .

Two regions have been defined for statistical analysis and bias, root mean square error and pattern correlations have been calculated for each. The effect of smoothing precipitation fields on statistics has been investigated. This investigation has been furthered by calculating fractions skill score curves, a novel method implemented recently for numerical weather prediction (Roberts & Lean (2008)). This method is new for climate analysis and comments on the usefulness of the method have been made, along with recommendations for future use.

Acknowledgements

There are many people that I owe a debt of gratitude to academically and non-academically - too many to name here. Thanks go to Len and Emily, who gave me everything I needed from my supervisors, and more.

Thanks go to my parents - Dad for showing me that nothing is broken which can't be fixed, and Mum for reminding me what's important when my head gets filled up with big ideas.

I gratefully acknowledge NERC for their financial support, without which I would have been unable to undertake this course.

Last but not least I thank my coursemates at Reading, who have been a big part in making this year one of my best so far. Writing this dissertation was (almost) a breeze with the company in room 105. Having others to share the tea-making burden with helped me get through some of the harder bits - sorry if I drank more than I made!

To those who do not know mathematics it is difficult to get across a real feeling as to the beauty, the deepest beauty, of nature ... If you want to learn about nature, to appreciate nature, it is necessary to understand the language that she speaks in. **- Richard Feynman**

I confirm that this is my own work and the use of all material from other sources has been properly and fully acknowledged.

. . . . . .

. . . . . .

List of Figures

Contents

Chapter 1

The Middle East

The Middle East is considered the world's most water-scarce region (Brown & Crawford (2009)). Water availability is important for human health and economic activity and in many places demand for water already outstrips supply. Current climate models predict that in the future the region will experience a decrease in precipitation leading to a decrease in river runoff in the region (Evans (2008), Kitoh et al. (2008)). Whilst models agree on the direction of the changes in the water cycle, they do not agree on the magnitude of these changes (Milly et al. (2005)). This may be partly because the region has a sharp spatial gradient in climate types as well as a highly varied landscape. The landscape and the climate interact in a complex way which makes modeling future climate in the region a challenge for climate models (Evans (2004)). One potential way of improving the skill of climate predictions in the region is to increase model resolution, which gives advantages such as better representation of weather systems and more accurate topography. The effect of model resolution on representation of climate is a main focus of this study. In this chapter the geography and the climate of the region are discussed, along with current model predictions for future climate of the region. The questions relating to modeling the climate of the

region which will be addressed in this study are also set out.

1.1 Geography

A map of the Middle East is shown in figure 1.1. The region has a varied landscape, from the Taurus mountains in Turkey and the Zagros mountains in Iran to the deserts of Syria, Iraq, Jordan and Saudi Arabia. Surrounding the region are several large bodies of water, moving clockwise from the eastern coast of the Mediterranean; the Black Sea, the Caspian Sea, the Persian Gulf and the Red sea.

Figure 1.1: *A map of the Middle East, modified from GoogleEarth (2009)*

Three main rivers run through the region and provide water to many communities. The River Jordan is fed by tributaries from the countries surrounding northern Israel and travels southwards along the boundary between the West Bank and Jordan to the Dead sea. 70–90% of the water in the Jor-

dan is used for human purposes, which has caused a large reduction in flow of the river. Coupled with the high evaporation rate, this means that the Dead sea is drying up (Klein & Flohn (1987)).

The two other major rivers in the region are the Tigris and the Euphrates, which descend from the slopes of the Taurus mountains in Turkey into Syria and Iraq before discharging into the Persian Gulf. These rivers define Mesopotamia, also known as the "'Cradle of Civilization'. This area saw the development of some of the earliest human civilizations, in no small part due to its rich, fertile soils – hence the name 'The Fertile Crescent'. It has now all but dried up, with much of the land cover transformed into bare land and salt crust, and it is on the WWF list of critical/endangered ecoregions (Olson & Dinerstein (2002)). Human activity is a major factor behind this degradation – water diversion for agricultural irrigation and construction of many dams in the headwaters of the Tigris and Euphrates have caused a reduction in their annual flow (Partow (2001)). This combination of stress on a fresh water source and rapid population growth substantially increases the vulnerability of the region to future climate change (Evans (2008)).

1.2 Climate

The Middle East has a Mediterranean macroclimate, characterized by cool, wet winters and hot, dry summers. Nearly all precipitation falls in winter, the dominant mechanism being eastward moving cyclones from the Mediterranean. The locations of precipitation are strongly influenced by surrounding mountains (Smith et al. (n.d.)). There are five dominant regions of precipitation associated with mountain ranges;

- The Mediterannean coastal range including the hills of Lebanon.
- The Taurus mountains of Turkey.

- The Zagros mountains of Iran.
- The Pontic range by the Black Sea.
- The Elburz range by the Caspian Sea.

Precipitation patterns are also influenced by the location of water bodies adjacent to the mountains. The Black and Caspian Seas, and eastern coast of the Mediterranean act as water sources for orographic precipitation. The Red Sea and Persian Gulf act as powerful sources of water vapour, however they trigger little precipitation locally due to the descending air in the Hadley cell (Evans (2004)). Water bodies are also a source of sea–breeze related precipitation, whereby unequal heating of land and sea generates a pressure difference which produces a wind component moving toward the land during the day, bringing with it moisture from the sea.

The mountains have a further indirect effect on precipitation. Through elevated heating they generate atmospheric subsidence that warms and dries the surrounding areas (Broccoli & Manabe (1992)), and it has been shown that summer subsidence forced by the Iranian Plateau adds extra warming and drying to Mesopotamia (Evans (2004)). This drying of surrounding areas partially explains the existence of deserts in the region. The desertification of the region can also be attributed to remote larger-scale climate behaviour such as the 'monsoon-desert mechanism' (Rodwell & Hoskins (1996)), in which diabatic heating in the Asian monsoon region induces a Rossby-wave pattern to the west which acts in combination with descending air in the Hadley cell to inhibit precipitation in the region. This is a factor behind the extremely dry summer climate, as the Asian monsoon peaks during this period (Rodwell & Hoskins (1996)).

There is a high temporal as well as spatial variability in rainfall in the Middle East. There is day to day variability in winter due to individual storms passing through the region. There is also the large annual variability from its

maximum in winter to almost no precipitation in summer. Furthermore there are interannual and decadal variations in precipitation, which reflect the far–field influence of the North Atlantic Oscillation (NAO) (Cullen et al. (2002)). The NAO is the dominant mode of Atlantic sector variability, and can account for 20–60% of the total variance in winter precipitation in Europe and the Mediterranean over the last 150 years. It has been shown that the first principal component of winter streamflow variability from the main Middle Eastern rivers reflect changes in the NAO, with positive phases of the NAO associated with reduced precipitation in the region (Cullen et al. (2002)). The El Niño/Southern Oscillation (ENSO) phenomenon, a dominant source of interannual climate variability over much of the globe, appears to have either an inconsistent (Ropelewski & Halpert (1987)) or weak (Halpert & Ropelewski (1992)) influence on the region. However there is evidence that the teleconnection of ENSO has extended its reach into the Middle East in recent decades (Price et al. (1998)).

The complex relationship between the landscape and climate as well as the temporal and spatial variability in precipitation makes modeling precipitation in the Middle East a challenge for climate models. Compared with many places in the world, the region is a data-sparse area which makes it harder to validate models. As such, only a relatively small body of work exists concerning regional climatic phenomena (Evans (2004)). However several studies forecasting change in the climate regime for the region have been performed, the general consensus of these is described in the next section.

1.3 Climate change predictions

Climate models predict that in the future the climate of the Middle East will be hotter and drier (Brown & Crawford (2009)). They predict that by the middle of the century the region will get warmer across all seasons, with

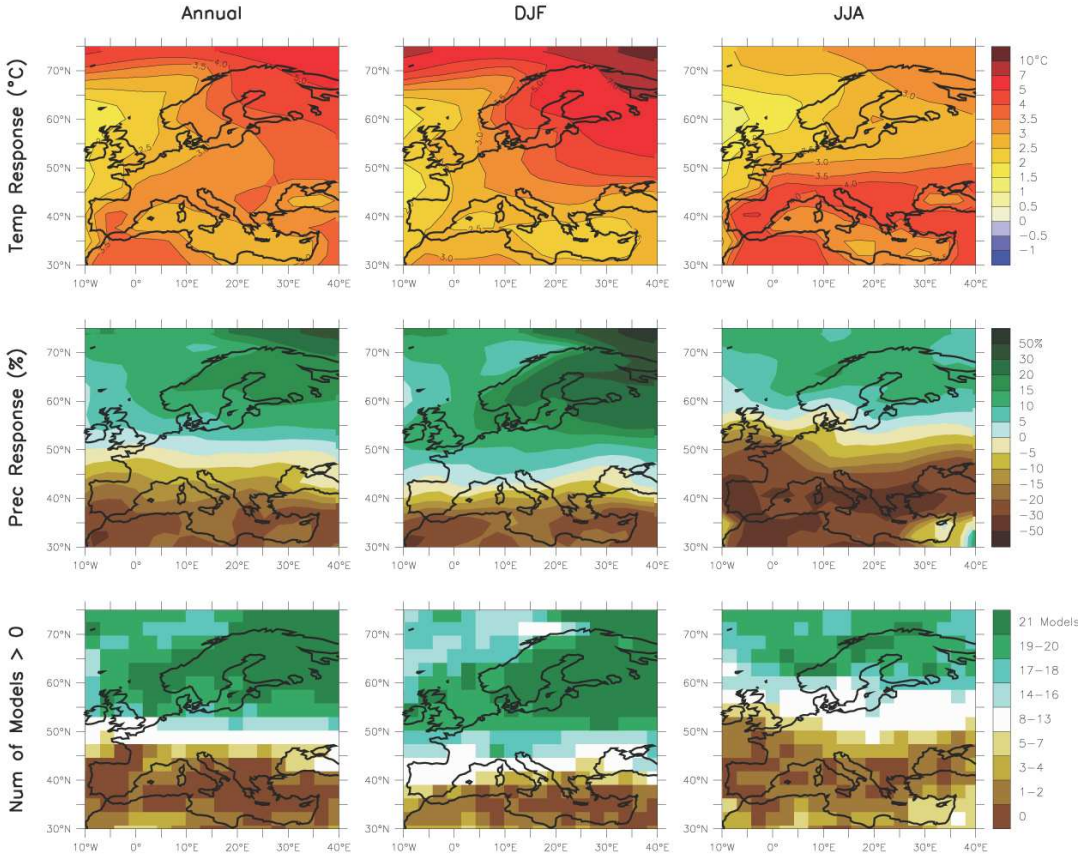

Figure 1.2: *Temperature and precipitation changes over Europe and the Mediterranean from A1B (high emission) simulations. Top row: Annual mean, DJF and JJA temperature change between 1980 to 1999 and 2080 to 2099, averaged over 21 models. Middle row: same as top, but for fractional change in precipitation. Bottom row: number of models out of 21 that project increases in precipitation (Christensen et al. (2007))*

an increase of between 1.5 to 3.7°C in summer and 2.0 to 3.1°C in winter (predictions based on climate models used in the recent Intergovernmental Panel on Climate Change (IPCC) report, ranging between lowest and highest greenhouse gas emissions scenarios, Cruz et al. (2007)). Higher temperatures will change patterns and amounts of precipitation - shown in figure (1.2) are projected changes in temperature and precipitation in the 21st century over Europe under an A1B (high emission) scenario (Christensen et al. (2007)). Models predict that the region including the Mediterranean, stretching from the strait of Gibraltar eastwards to Turkey and the Middle East will get drier. In the Middle East significant rainfall declines in winter will outweigh slight increases during the dry summer (Cruz et al. (2007)). One study has predicted that future precipitation reduction will be sufficient that the Fertile Crescent will lose its current shape and may even disappear (Kitoh et al. (2008)). The NAO is also predicted to become more positive in a future climate, which would further decrease winter rainfall Cullen et al. (2002).

The region is also set to experiencE an increase in extreme rainfall events (Alpert et al. (2008)). It is predicted that the dominant precipitation mechanism will shift from direct dependence on storm tracks and toward greater precipitation triggering by upslope flow of moist air masses (Evans (2009)). This is in agreement with the predicted reduction in the strength of the Mediterranean storm track in a future climate (Bengtsson & Hodges (2006)). Furthermore there may be small northward movement of the intertropical convergence zone (ITCZ) which would change the atmospheric stability over the Saudi desert and could trigger increases in precipitation in some areas (Evans (2009)).

When combined with population pressures and already strained water resources, these future predictions of precipitation reduction in vital hydrological areas do not paint a good picture for the people of the region in the next century. However, forewarned is forearmed and increases in reliability and accuracy of climate change predictions will help management of a

dwindling resource. This study focuses on precipitation in climate models and specifically how the current trend toward higher spatial resolution will improve the accuracy of precipitation predictions. The questions upon which this study focus are laid out in the next section.

1.4 Aims of the study

There are many conceptual models of the climate, ranging from simple radiation budget models which can predict an average global equilibrium temperature, up to spatially and temporally discretised global circulation models. Predictions of climate change come primarily from coupled ocean-atmosphere global climate models (Thorpe (2005)). These are mathematical models, the most basic of which solve the fluid equations of motion for the atmosphere on a 3 dimensional grid over time (climate models are described in more detail in chapter 2). The size of grid upon which the equations are solved varies between models and is of vital importance. Too low a resolution and weather systems cannot be adequately resolved; too high and the computing cost can become prohibitive.

In this report the output from two high resolution models for the Middle East is studied. One is HiGEM, a global coupled model developed by the Natural Environment Research Council (NERC), the UK academic community and the Met Office Hadley Centre. The other is an atmosphere only regional climate model (RCM), based on the PRECIS regional climate modeling system, developed at the Hadley Centre. The aims of this study are as follows:

- To evaluate the performance of the two climate models in representing rainfall over the Middle East
- To use statistical measures to quantitatively evaluate model skill

- To investigate how the variation of model skill with resolution might be represented

In the next chapter the theory and basic ideas behind climate modeling are discussed, along with a more complete description of the two models used in this study as well as the observations used for comparison.

Chapter 2

Model description and observations

Climate models have varying levels of complexity, ranging from simple radiation budget models, through to basic atmosphere only models to Earth system models which include components for the ocean, the cryosphere, the biosphere and more. They are widely used to understand and predict the evolution of the climate and have recently been the key to attributing recent change in climate to human activities (Slingo et al. (2009)). Before climate models are used for prediction however, they must be validated against past observations to verify that they are representing the climate system accurately.

The focus of this chapter is climate modelling and the different types of models used. The importance of model resolution for the representation of climate is discussed. Finally the two models used in this study are described, as well as the different observational datasets used for validation against the models.

2.1 Climate Modelling

A climate model is an attempt to represent the many processes that produce climate in a mathematical model. The aim is to understand these processes and predict the effects of changes in interactions. This is accomplished by describing the system in terms of basic physical principles, reduced to mathematical laws, which can be numerically solved on a spatial grid (McGuffie & Henderson-Seller (2005)). General circulation models (GCMs) are one kind of model, which incorporate the three–dimensional nature of the atmosphere by discretising in space and time. They can be either atmosphere only (AGCM) or ocean only (OGCM) whereby interactions with the missing component of the system are forced externally. However many state of the art climate models are fully coupled, they have atmospheric and oceanic components and interactions between them are generated internally by the model.

The fundamental laws solved in GCMs are conservation laws: conservation of energy, conservation of momentum and conservation of mass. The ideal gas law is also solved, and dynamics are described by the primitive equations (an approximated form of the navier–stokes equations) on a rotating sphere. Generally equations are solved to give the mass movement (i.e. wind field or ocean currents) at the next timestep, but models also include processes such as cloud and sea ice formation and heat, moisture and salt transport (McGuffie & Henderson-Seller (2005)). Some components of the climate system such as convective clouds, cloud microphysics and subgrid scale eddies occur on too small a scale to be resolved explicitly by climate models and so are represented in models by simplified mathematical formulae (Peixoto (2007)). This is known as parametrization.

Similar to GCMs are regional climate models (RCMs), which generally use the same equations as GCMs but are applied over a limited area, rather than the whole globe. Because they do not model the whole globe they are less

computationally expensive and so are able to operate at higher resolutions and generate high resolution output for studying global change (Wang et al. (2004)). At their boundaries they are generally 'driven' by a GCM or by observed data, whereby fields at the lateral boundaries are given the same values as the driving GCM/observational data.

2.1.1 Model Resolution

Climate modelling grew out of numerical weather prediction (NWP) more than 40 years ago. Since then climate models have become increasingly complex with extra components of the climate system being added. Because of this, unlike NWP models which have steadily increased in spatial resolution, until recently climate models have still operated on regular grids of the order 200–300km (Slingo et al. (2009)). At this scale models cannot adequately resolve weather systems such as mid–latitude fronts and tropical cyclones. However improvements in computing capability mean that higher resolution models have recently developed and are becoming more common (Slingo et al. (2009)).

Increasing the resolution of climate models means that weather systems are better represented (Catto et al. (2009)). Higher resolution in the atmosphere and ocean has been shown to allow coupling to occur on small spatial scales, and small scale interactions can be more realistically captured (Shaffrey et al. (2009)). This, along with other high resolution benefits such as more detailed orography will hopefully result in more accurate representation of precipitation processes in climate models. The hope is that climate will be more accurately represented through better representation of weather systems, regional circulation, topography and heterogeneity in land cover. Representation of topography is particularly important in the Middle East for precipitation due to the presence of mountains and the orographic precipitation associated with them. The topography of the region is shown in

figure 2.1, along with the topography as it is represented by the two models used in this study.

Whilst the move towards higher resolution goes on (some atmosphere-only models now operate at resolutions of 20km (Kitoh et al. (2008))), it may be that the cost of the extra computing power will outweigh the increase of skill gained by moving to higher resolutions. In NWP this is especially a problem since a move to smaller scales results in forecast errors growing more rapidly, and so higher resolution many not give any significant increase in model skill (Lorenz (1969), Done et al. (n.d.), Mass et al. (2002)). Because of these issues, a new scale-selective method for evaluating NWP precipitation forecasts has recently been introduced (Roberts & Lean (2008)). This novel method has been modified in this study and implemented to the output of climate models rather than NWP models. The theory is discussed in section 4.2.

2.2 Description of models

Two models are used in this study; HiGEM, an atmosphere–ocean coupled GCM, and an atmosphere–only RCM. The main differences in the models are detailed in table 2.1. Further details of the models are described below.

2.2.1 HiGEM

HiGEM is a global coupled model, developed by NERC, the UK academic community and the Met Office Hadley Centre. It based on the latest configuration of the UK Met Office Unified Model, HadGEM1 which contributed to the IPCC 4th Assessment Report (Solomon et al. (2007)).

The horizontal resolution of HadGEM1 is 1.875° x 1.25° in longitude and latitude in the atmosphere, and 1° x 1° (increasing to 1/3° meridionally near

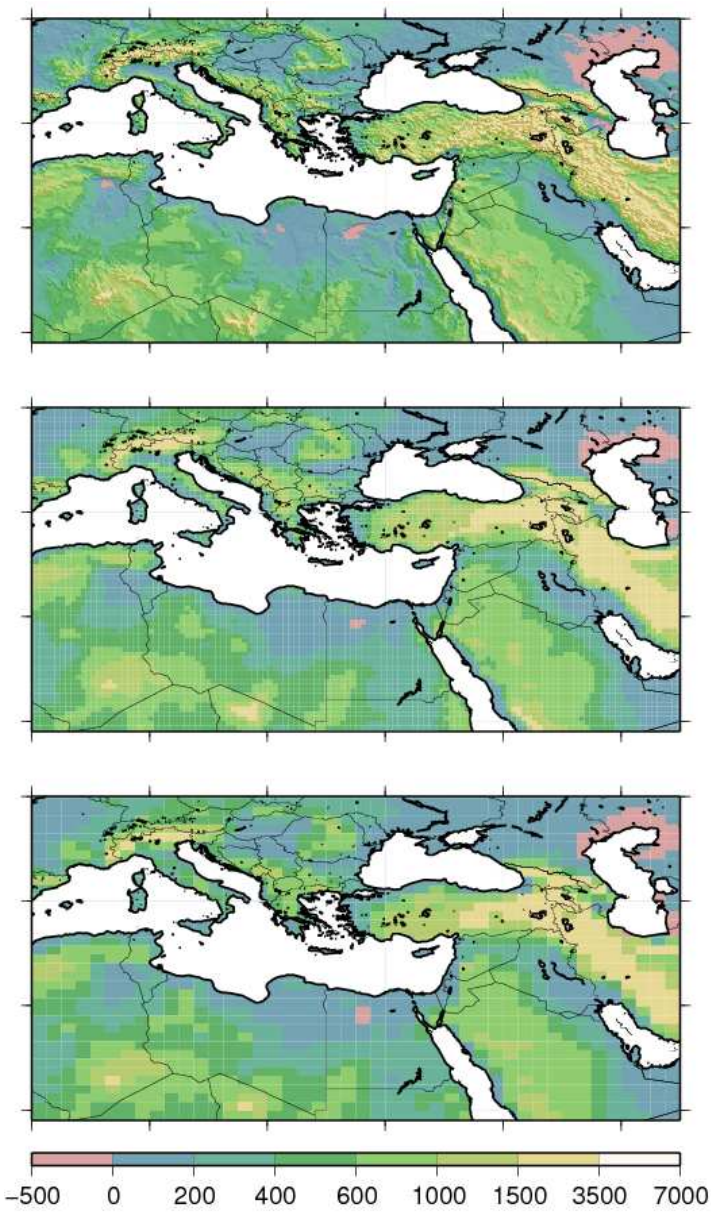

Figure 2.1: *Topography of the region (top), as represented by the regional model (middle) and by HiGEM (bottom). Units are m.*

	HiGEM	Regional Model
Region	Whole globe	Europe, Mediterranean & Middle East
Components	Coupled atmosphere and ocean	Atmosphere only
Resolution	1.25° x 0.83° for atmosphere 1/3° x 1/3° for the ocean	0.44° x 0.44°
Vertical levels	38 in atmosphere, 40 in the ocean	19
Lateral boundary conditions	None needed	From HadAM3P

Table 2.1: *Comparison of the two models used in this study.*

the equator) in the ocean. In HiGEM this has been increased to 1.25° x 0.83° in longitude and latitude for the atmosphere, and 1/3° x 1/3° globally for the ocean and sea ice. The timestep of the model is 20 minutes (Shaffrey et al. (2009)).

The atmosphere of HiGEM has 38 levels in the vertical. The top of the model is at 39km, which means the stratosphere is not well resolved. The ocean component has 40 unevenly spaced levels in the vertical with enhanced resolution near the surface to better resolve the mixed layer and atmosphere-ocean interaction processes. The maximum ocean depth is 5500m (Shaffrey et al. (2009)).

The orography is derived from the 1' GLOBE dataset, which provides an accurate representation of the mountains and their sub-gridscale characteristics (Shaffrey et al. (2009)). The topography as it is represented in HiGEM

is shown in figure 2.1.

Climatologies are based on years 21–70 of a model run, so that the upper ocean and atmosphere have sufficient time to spin up. Initial conditions have been given to the model to simulate climate over the past half century.

2.2.2 The Regional Climate Model

The RCM used in this study is based on PRECIS, a model based on HadAM3P, a global, atmosphere-only model developed at the Hadley Centre. The RCM has a horizontal resolution of 0.44°, giving a grid spacing of 50km. This permits a large domain to be used whilst representing significantly more topographic variation than is possible in the 200km scale of the generation of climate models used in IPCC (Black (2009), Slingo et al. (2009)) (topography as represented by the RCM is shown in figure 2.1). The model has 19 levels in the vertical and includes the whole Mediterranean so that cyclones which bring most of the rain to the Middle East do not travel through the domain boundary (Black (2009)). The domain of the model is shown in figure 2.2. It should be noted that there are normally problems associated with model output close to the boundary, therefore when the RCM will be evaluated only output at some distance from the boundary will be looked at.

RCMs are applied over a limited area and so require input at both the surface and lateral boundaries of the domain. Lateral boundary conditions were derived from integrations of HadAM3P forced with surface boundary conditions (sea surface temperature, sea ice fraction), which were derived from observations. Boundary conditions for the PRECIS RCM are on a grid of 2.5° latitude x 3.75° longitude, about 300 km resolution at 45N or 400 km at the equator. Surface boundary conditions for the RCM are based on HadCM3 predictions and observations (Black (2009)).

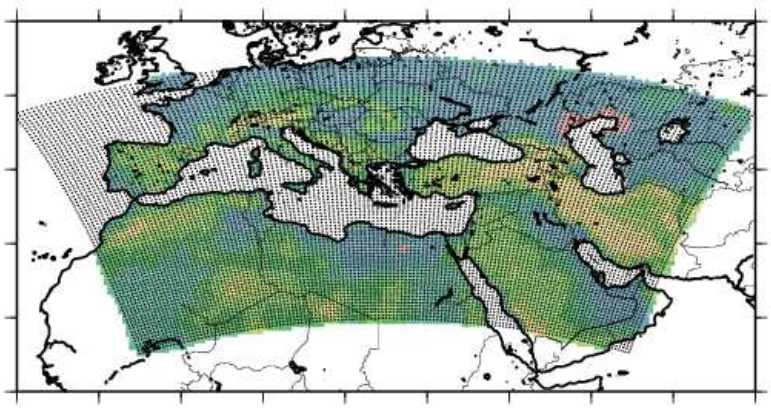

Figure 2.2: *The domain over which the regional model is evaluated.*

2.3 Description of observations

Compared with many places in the world, the Middle East is a data sparse area (Evans (2004)). As such, several different observational datasets, each with their own advantages and disadvantages, have been used.

The global precipitation dataset from the global precipitation climatology centre (GPCC) is used. This data is based upon quality controlled ground station data from up to 43,000 stations, with irregular coverage in time. These provide a 1° x 1° resolution precipitation climatology for the period 1951 to 2004 (Earth System Research Laboratory (2009)).

Global precipitation climatology project (GPCP) data are also used. This consists of data from over 6,000 rain gauge stations, satellite geostationary and low-orbit infrared, passive microwave, and sounding observations which are merged to estimate monthly rainfall on a 2.5° global grid from 1979 to the present (NASA Goddard Space Flight Center (2009)).

Finally, observations from the tropical rainfall measuring mission (TRMM) satellite are used. This satellite gives a fine spatial resolution of precipitation (0.25° x 0.25°) around the globe from 50° N to 50° S. Climatologies are calcu-

lated from 1997 to 2007 and consist of TRMM observations constrained with gauge station and GPCP data (Huffman, G.J. and Adler, R.L. and Bolvin, D.T. and Gu, G. and Nelkin, E.J. and Bowman, K.P. and Hong, Y. and Stocker, E.F. and Wolff, D.B. (2007)).

To compare mean sea level pressure and wind fields in the models, data from ERA-40 reanalysis was used. ERA reanalysis is a dataset created by assimilating many sources of observations into the ECMWF climate model at a 40km resolution (Uppala et al. (2005)).

Chapter 3

Visual comparison of climatologies

HiGEM and the Regional Climate Model have been run to produce climatologies over the Middle East. These climatologies give average values of meteorological variables for the domains over which they are run. Although the focus of this study is specifically to investigate how well the models represent precipitation, it is important to evaluate how well the models represent other aspects of the climate system. This is because there are different climatological processes that cause precipitation and so how a model represents precipitation is dependent on how well it represents these processes, which are dependent on other meteorological variables.

In this chapter model climatologies for precipitation, 10m surface wind fields and mean sea level pressure are plotted and visually compared to climatologies taken from a variety of observations. Several observational datasets for precipitation have been plotted which have their own advantages and disadvantages; these are discussed.

3.1 Precipitation

3.1.1 Comparing observations

Shown in figure 3.1 are observed precipitation climatologies. (a) and (b) show boreal winter (DJF) and summer (JJA) observations from the GPCC dataset (Earth System Research Laboratory (2009)). White areas are shown over land because the data is taken from rain gauge and gauge station data and no data is available over the sea. Shown in (c) and (d) are DJF and JJA climatologies taken from the GPCP dataset (NASA Goddard Space Flight Center (2009)) - the dataset based on gauge station, satellite and sounding observations. Finally in (e) and (f) DJF and JJA climatologies from the TRMM satellite are shown (Huffman, G.J. and Adler, R.L. and Bolvin, D.T. and Gu, G. and Nelkin, E.J. and Bowman, K.P. and Hong, Y. and Stocker, E.F. and Wolff, D.B. (2007)). N.B. For a more detailed description of observation datasets see section 2.3.

All observations show that in the Middle East region there is a strong seasonal cycle of precipitation - precipitation falls predominantly in winter, with little observed in summer. The pattern of precipitation in winter has similarities in all observations; a band of rainfall around the southern and western coast of Turkey with some precipitation falling over the Black Sea. In summer the rainfall is minimal except in a single area around the eastern edge of the Black Sea which can be seen in all three sets of observations. Observations also show the West African monsoon to the south in summer, the large band of rainfall stretching from the equator to 15°N.

There are some significant differences in the observations however; GPCC and TRMM both show a relatively intense band of rainfall falling along the eastern edge of the Mediterranean in winter which does not appear in the GPCP dataset. Whilst this may seem like a small difference, it is of vital importance for impacts studies since this wintertime rainfall is real

and can be seen from rainfall gauge data (Sharon & Kutiel (1986), Black (2009)). In particular it falls along the length of the Jordan river, upon which many communities depend heavily. Moving eastward from the Mediterranean across Israel and towards the desert there is a sharp gradient in rainfall contour lines, which is almost totally absent in the GPCP data. It is for this reason, along with the fact that GPCP has the lowest resolution of all observations, that the GPCP data will not be used for statistical comparison with the models – attempting to verify a model against observations is a misleading exercise if the observations do not match reality in important areas. The GPCC and TRMM datasets show generally the same pattern of precipitation – they both show the rainfall falling near the Jordan river, they both capture the orographic precipitation in Taurus mountains of South Eastern Turkey where the Euphrates and Tigris begin their journey toward the Persian Gulf and they both capture the wintertime rainfall over the Fertile Crescent.

The GPCC dataset however does not have data over the seas since it comes only from ground stations. It also has a lower resolution than TRMM, which shows a more detailed pattern of precipitation. Conversely, the TRMM climatology is calculated over the shortest time period (1997–2007) whereas the GPCC and GPCP data stretch back over longer time periods (starting from 1951 and 1979 respectively). It is thought however that when it comes to statistical analysis, the advantages of TRMM over the other datasets outweigh the disadvantage of having been calculated over a shorter time period. The TRMM data will therefore be used for model validation.

3.1.2 Looking at the models

Shown in figure 3.2 are precipitation climatologies for the models. (a) and (b) show DJF and summer JJA climatolgoies calculated by HiGEM. (c) and (d) show DJF and JJA climatologies calculated by the RCM. HiGEM fields

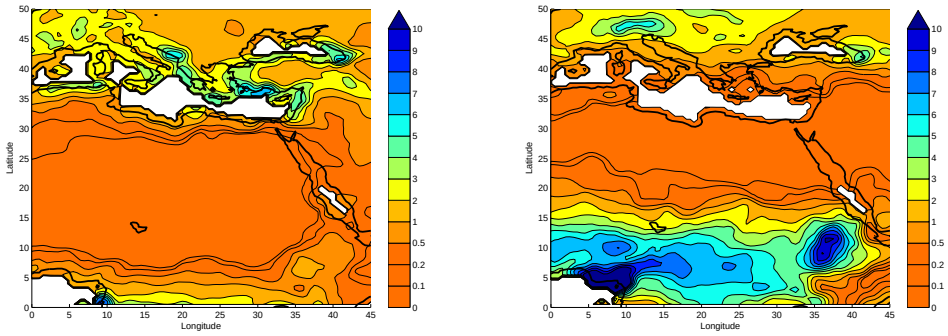

(a)

(b)

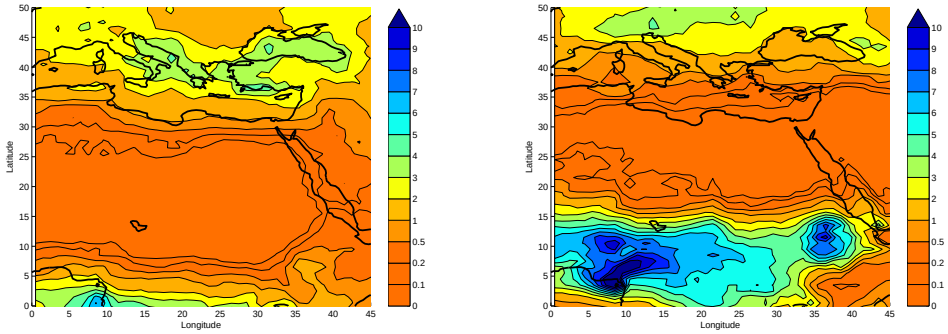

(c)

(d)

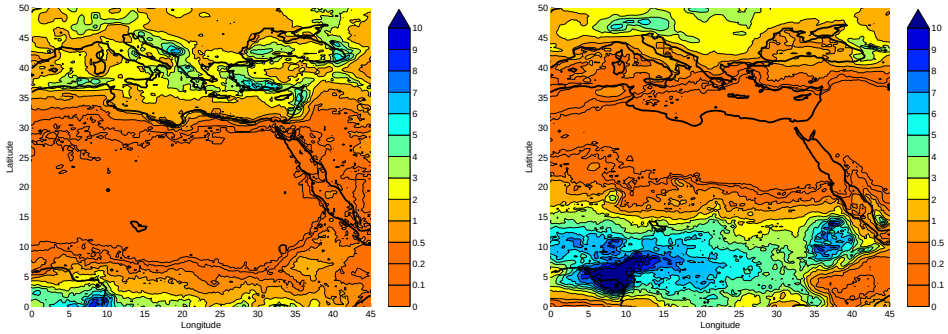

(e)

(f)

Figure 3.1: *Precipitation climatologies from observations. Figure (a) and (b) show boreal winter (DJF) and summer (JJA) climatologies from the GPCC dataset. (c) and (d) show DJF and JJA climatologies from GPCP data and (e) and (f) show climatologies from TRMM. Units are in mm day*$^{-1}$*. The lack of observations over the ocean in the GPCC climatologies is due to observations having been taken from ground stations only.*

are smoother than the RCM due to the lower resolution of the model and the extent of the RCM fields show the spatial limits of the modelled area.

Both models capture the seasonal cycle in precipitation with all rainfall falling in winter and little in summer. They also both capture the general shape of the winter precipitation around the coastlines of Turkey and to some extent the small area of summer rainfall over the Eastern coast of the Black Sea – in the RCM this is present, but lower than that seen in either HiGEM or observations.

HiGEM however overestimates precipitation around the south/south eastern coast of Turkey and slightly overestimates it over the Fertile Crescent. The RCM has significantly less precipitation in the region compared to observations, especially at the coasts.

Both models capture some amount of detail of the gradient of the precipitation contours around the eastern Mediterranean – HiGEM shows the gradient as slightly sharper than observations (TRMM & GPCC), whereas the gradient in the RCM is slightly smaller due to the underprediction of precipitation on the coast.

3.2 Mean Sea Level Pressure

Shown in figure 3.3 are mean sea level pressure (mslp) climatologies from observations and from models. The observations in this case are taken from ERA–40 reanalysis. Looking at the ERA–40 reanalysis in (a) and (b) the general pressure patterns can be determined.

In winter there is a region of high pressure to the east and south east of Turkey. There is also a region of low pressure stretching from between Crete and Cyprus. This is known as the Cyprus Low (Alpert et al. (2005)), which is associated with weather systems moving eastwards towards the coast of

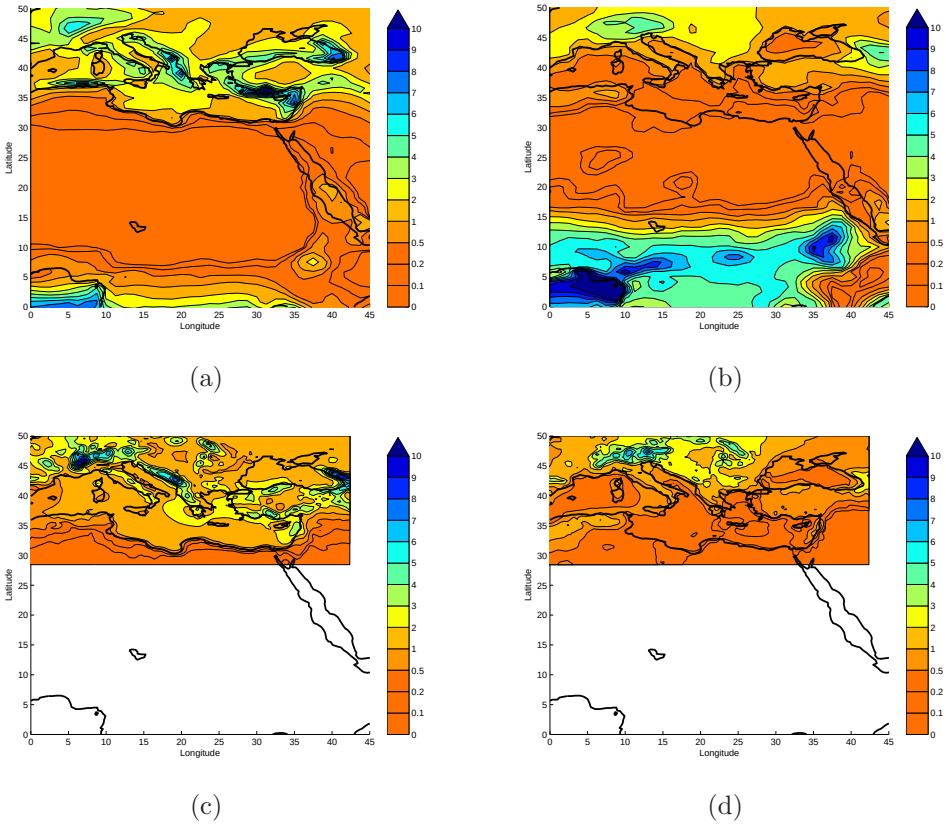

Figure 3.2: *Precipitation climatologies calculated by the models. Figure (a) and (b) show DJF and JJA climatologies calculated by HiGEM. (c) and (d) show DJF and JJA climatologies calculated by the RCM. Units are in mm day^{-1}. Note the cut-off in the RCM climatologies limit of the model output looked at in this study.*

the Mediterranean, bringing wintertime rainfall.

In summer the pressure drops, and the pattern observed is a region of low pressure eastwards towards the Persian Gulf, which increases rapidly northwards and westwards creating a high gradient of pressure associated with high wind speeds through geostrophic balance. A long tongue of low pressure can also be seen in summer, extending westwards from Northern Iraq towards Cyprus and over the Mediterranean. HiGEM pressure fields are shown in 3.3(c) and 3.3(d). It captures the pressure patterns fairly well; the general pattern of high–low pressure between the North East of the domain and Cyprus can be seen. It also captures some of the spatial shape of the summertime low pressure tongue.

The Cyprus Low is represented in HiGEM, although its spatial extent and intensity is underestimated in the model. The maximum of the low appears over the South West coast of Turkey, with a pressure of one or two millibars greater than that from ERA. The pattern of summer pressure is captured well, the shape of the sharp gradients is represented accurately, however the intensity of the low pressure east of the Mediterranean is less intense than ERA.

RCM pressure fields are shown in 3.3(e) and 3.3(f). The RCM captures summer pressure patterns well, both in shape and intensity. Winter patterns however do not show the intensity of the high pressure over Turkey and it can be seen that the Cyprus Low is not well represented in the model climatology.

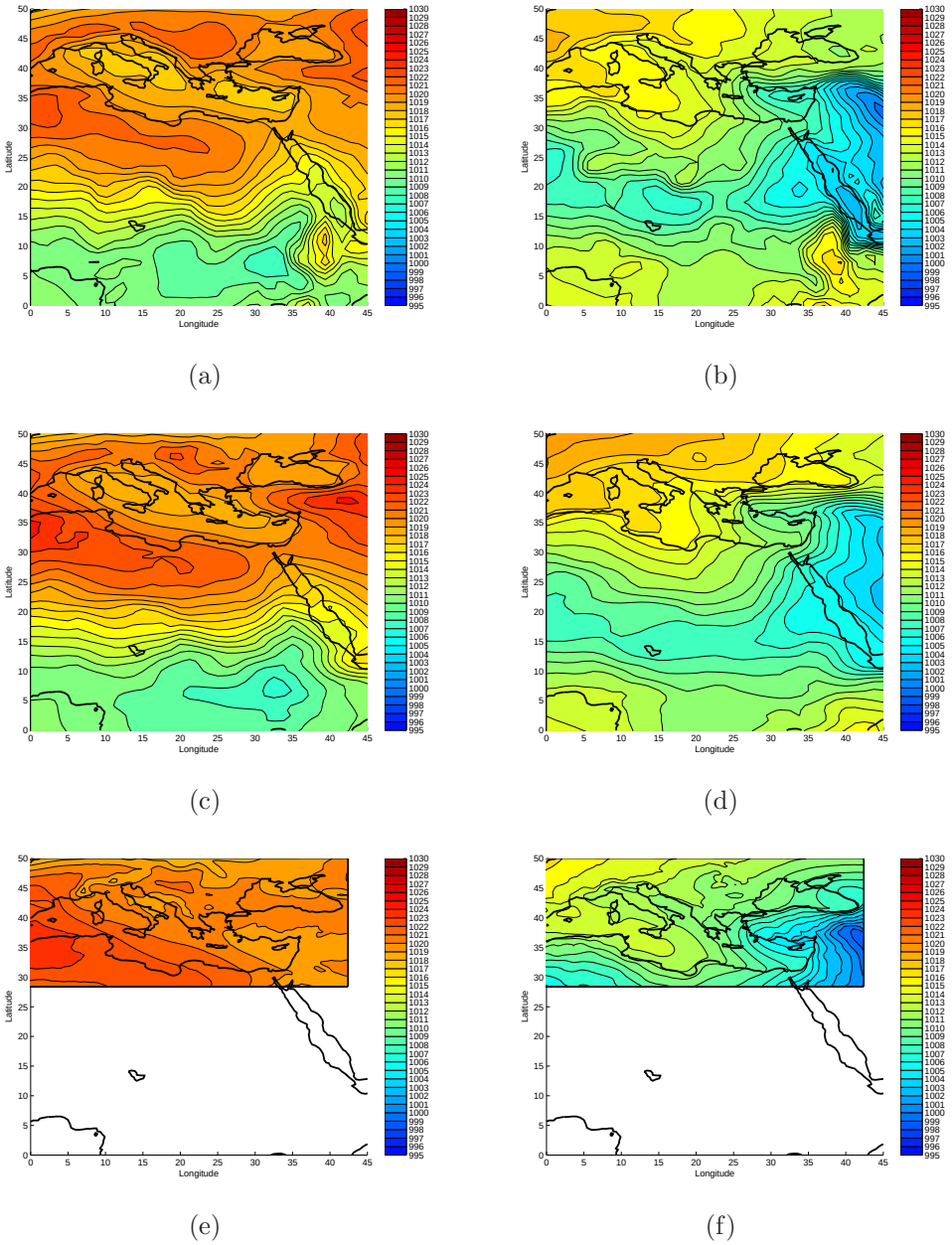

Figure 3.3: *Mean Sea Level Pressure climatologies from observation and models. Figure (a) and (b) show DJF and JJA climatologies from the ERA-40 reanalysis. (c) and (d) show DJF and JJA climatologies calculated by HiGEM and (e) and (f) show climatologies from the RCM. Units are millibar, contours are spaced 1mb apart.*

3.3 Surface Wind Patterns

3.3.1 Observed Wind Fields

Shown in figure 3.4 are climatological 10m surface wind patterns from observations and from models. The observations for DJF and JJA are from ERA-40 reanalysis and are shown in (a) and (b).

The observed winter wind field show relatively low speeds over the much of the land of the Middle East. Strong westerly winds can be seen over the Mediterranean. This is the Mediterranean storm track. Where this meets the land there is slight north easterly flow, which, upon meeting the moist air from the Mediterranean generates convergence and ascent. Since this air holds moisture from passing over the sea, precipitation results, which is observed in this general area. Relatively strong northerly winds are also observed over the Aegean. Winds are generally stronger since the sea surface is generally smoother than the rougher land surface, so winds passing over the sea experience less friction.

The wind patterns are also consistent with the pressure patterns, with wind moving counter-clockwise around the Cyprus low in winter. This can be seen in the westerly Mediterranean storm track and also in the south westerly movement of air over the land to the east of the Mediterranean. There is no corresponding easterly flow to the north however, this could possibly be due to the presence of the Taurus mountains which would hinder any horizontal movement of air.

In summer the wind also follows the pressure patterns, moving counter-clockwise around the strong low pressure area, with greater speeds due to the stronger presssure gradient. Winds over the Mediterranean also have more of a northerly component than in winter. Furthermore, over Turkey the winds are northerly, whereas in winter there is no net wind.

There is also very strong northerly flow over north east Africa in summer; this movement of air away from the Mediterranean could be a factor behind the lack of precipitation; air carrying moisture is moving away from the region before it has a chance to cause precipitation. The air then flowing over the Middle East would then be fairly dry since it would not have travelled far over water.

3.3.2 Modelled Wind Fields

10m surface wind fields calculated by HiGEM for DJF & JJA are in (c) and (d) of figure 3.4 and results for the RCM are in (e) and (f). Fields calculating by subtracting ERA wind fields from model output are shown in figure 3.5. The direction and magnitude of the arrows in these plots show the direction and magnitude of the errors in the modelled fields.

HiGEM captures the general patterns in winter, however it underestimates the magnitude of winds in the Mediterranean storm track. It also fails to capture the northerly flow over the Aegean. It captures well however the north easterly convergence–causing flow in the south east of Turkey, which is in fact overestimated in the model which can be seen from the convergence in the errors seen in figure 3.5(a). This extra convergence would cause extra ascent in the model, which could well be a factor in the overestimation of precipitation seen in HiGEM in the area. The general summer flow is captured fairly well in HiGEM, however the strength of the Mediterranean storm track is underestimated. This could be associated with the underestimation in intensity of the low pressure patterns east of the Mediterranean described in section 3.2; less intense low pressure would cause a weaker circulation.

The RCM underestimates the strength of the Mediterranean storm track in winter. Furthermore, it overestimates the westerly flow east of the Mediterranean and shows a slight northerly flow over Turkey. These errors can be seen to diverge outwards from the region of precipitation, seen clearly in fig-

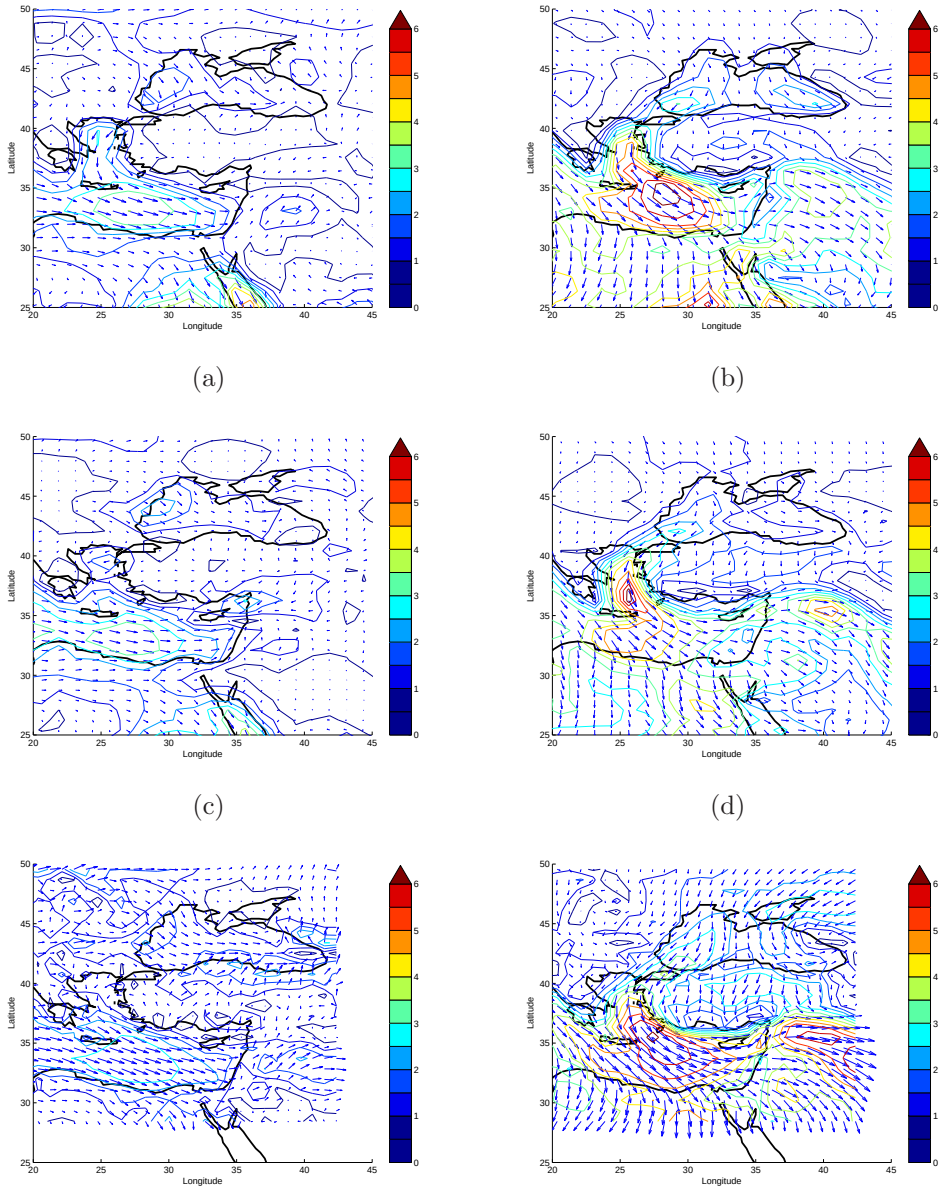

Figure 3.4: *Climatological 10m surface wind fields from observation and models. Figure (a) and (b) show DJF and JJA wind patterns from ERA-40 reanalysis. (c) and (d) show DJF and JJA wind patterns calculated by HiGEM and (e) and (f) show results from the RCM. Units are* ms^{-1}*, arrow sizes are proportional to wind speed.*

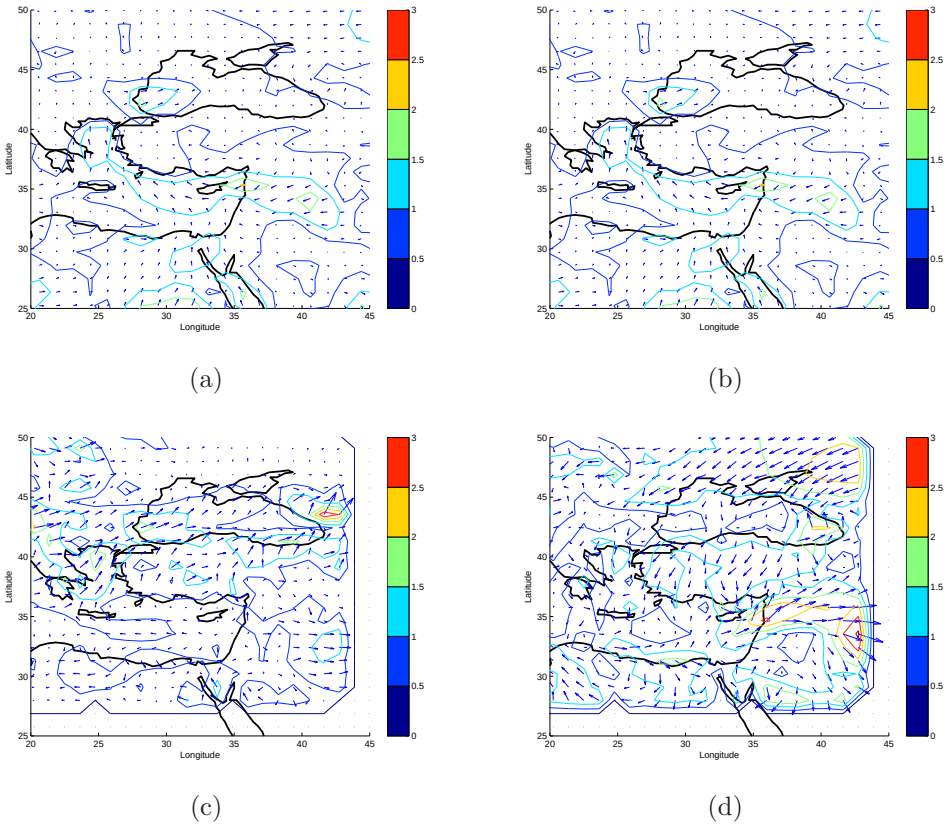

Figure 3.5: *Errors in 10m surface wind fields between models and ERA-40 reanalysis. Figure (a) and (b) show DJF and JJA wind field errors found by subtracting ERA fields from HiGEM. (c) and (d) show DJF and JJA wind field errors found by subtracting ERA fields from the RCM fields. Units are* ms^{-1}*, arrow sizes are proportional to wind speed.*

ure 3.5(c). This would cause a smaller convergence at ground level than is seen in observations, causing less ascent and therefore less precipitation. This is then potentially a factor in the lack of precipitation observed in the area, described in section 3.1.2. Errors are larger in summer, with the RCM predicting over–northerly flow over most of the domain. The overestimation of the magnitude of the westerly flow over the desert east of the Mediterranean is one of the two largest sources of error in the model, along with a north–easterly flow in the north–east of the domain, where the ERA reanalysis has almost no wind.

3.4 Discussion

Both models represent the seasonal cycle of precipitation well, and are successful in capturing the general spatial pattern. However HiGEM overestimates the total amount of precipitation and the RCM underestimates it. Both models also underestimate the magnitude of the winds making up the Mediterranean storm track which is associated with the Cyprus low, which is underestimated in HiGEM and even moreso in the RCM.

Both models have errors in wind fields around the main region of precipitation around the east coast of the Mediterranean, with HiGEM overestimating convergence in the region and the RCM underestimating it. This could well be associated with the errors in precipitation amounts; extra convergence in HiGEM would give extra ascent and so give too much precipitation, and a lack of convergence in the RCM would give less ascent and so less precipitation.

Visual comparison of climatologies has allowed a qualitative evaluation of model performance. However it is useful exercise to evaluate quantitative, statistical, measures of model skill to pin down specific areas of weakness or strength in the model. This is addressed in the following chapter.

Chapter 4

Statistical verification methods

The output from the two models has been compared visually with observations and qualitative distinctions have been drawn. Quantitative measures of differences between models and reality can be obtained by using statistical measures of skill. In this chapter several standard measures are described - the bias, the root mean square error and the pattern correlation. A new method for evaluating how model skill varies with spatial scale is also described. This has been adapted for climate modelling from a new method recently implemented by Roberts and Lean for numerical weather prediction (Roberts & Lean (2008)).

4.1 Statistical measures of model skill

Bias has been used to evaluate model performance against observations, it is calculated as

$$\text{Bias} = \bar{M} - \bar{O} \tag{4.1}$$

where $\bar{M}$ is the spatial mean of a modelled value over a domain and $\bar{O}$ is the spatial mean of observed values. This measures the amount by which

the model over or underestimates the average value of a parameter over a domain.

Root mean square error (RMSE) is given by

$$\text{RMSE} = \sqrt{\frac{1}{N}\sum_{i=1}^{N}(O_i - M_i)^2} \tag{4.2}$$

where N is the number of observed (O) and modelled (M) values being compared. Here N is the number of grid boxes in the domain. The RMSE is a basic measure of accuracy, with a lower value indicating a more accurate field

The pattern correlation is also used, which is the correlation of a series of data points from the observed field with corresponding values from the modelled field at a fixed time,

$$\rho = \frac{\sum_{i=1}^{N}(O_i - \bar{O})(M_i - \bar{M})}{\sqrt{\sum_{i=1}^{N}(O_i - \bar{O})^2}\sqrt{\sum_{i=1}^{N}(M_i - \bar{M})^2}}, \tag{4.3}$$

where sums are carried out over all grid boxes. A value of $\rho = 1$ represents a modelled field identical to observations, decreasing to $\rho = 0$ for no correlation.

4.2 Fractions Skill Scores

Higher model resolution does not necessarily mean better objectively scored accuracy (Roberts & Lean (2008)). In NWP this is especially a problem since a move to smaller scales results in forecast errors growing more rapidly, and so higher resolution many not give any significant increase in model skill (Lorenz (1969), Done et al. (n.d.), Mass et al. (2002)). Because of these issues, a new scale-selective method for evaluating NWP precipitation forecasts has recently been introduced (Roberts & Lean (2008)). Using fractions

skill scores this method allows determination of the spatial scales at which forecasts become skilful. It uses the concept of nearest neighbours as the means of selecting the scales of interest and is applied to thresholds. The result is a measure of forecast skill, Fractions Skill Score (FSS), against spatial scale for each threshold. This verification method described in their work is reproduced here.

4.2.1 Conversion to binary fields

Observed and modelled rainfall fields are first projected onto the same grid. In this case since the TRMM observations have a higher resolution, these are projected onto each of the model grids. A threshold (q) is chosen and used to convert the fields into binary fields (I_O) and (I_M). All grid points exceeding the threshold are assigned a value of 1 and all others a value of 0, i.e.,

$$I_O = \begin{cases} 1 & O_r \geq q \\ 0 & O_r < q \end{cases}$$

,

with a parallel result for I_M. An illustration of binary fields is shown in figure 4.1.

4.2.2 Generation of fractions

The binary fields are then converted to fractions. For every grid point in the binary fields obtained from equation (4.2.1) the fraction of surrounding points within a given square of length n that have a value of 1 (i.e. that have exceeded the threshold) is calculated. This is described for the observed field by

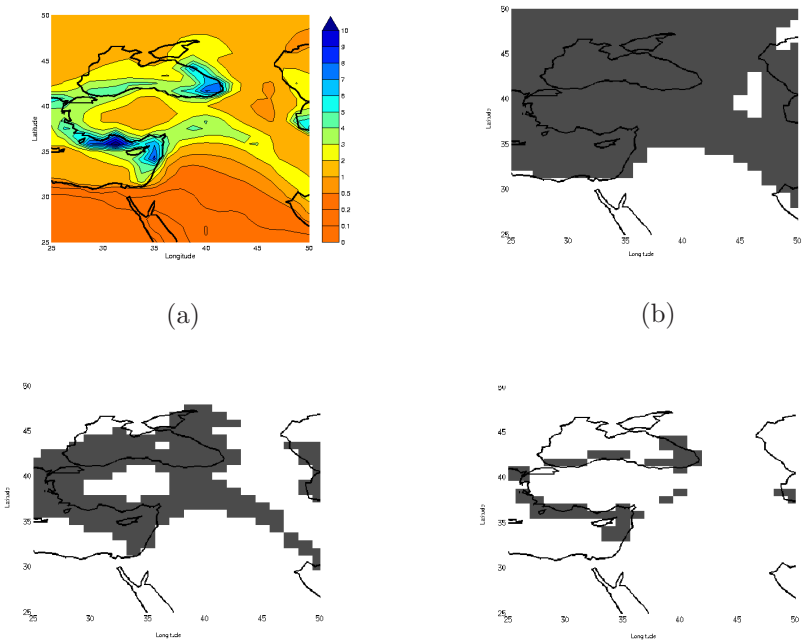

(a) (b)

(c) (d)

Figure 4.1: *Example binary conversion applied to winter precipitation output from HiGEM. Shown in (a) the model output and in (b) (c) and (d) are binary fields calculated for thresholds 1mm day^{-1}, 2mm day^{-1} and 4mm day^{-1} respectively (grey areas are 1's, white areas 0's).*

$$O(n)(i,j) = \frac{1}{n^2}\sum_{k=1}^{n}\sum_{l=1}^{n} I_0\Big[i+k-1-\frac{(n-1)}{2}, j+l-1-\frac{(n-1)}{2}\Big], \quad (4.4)$$

with a similar result for the modelled fractions, $M_{(n)}(i,j)$. Here i goes from 1 to N_x, where N_x is the number of columns in the domain and j goes from 1 to N_y, where N_y is the number of rows.

This creates a resultant field of observed fractions, $O_{(n)}(i,j)$, for a square of length n obtained from the binary field I_O and a similar field $M_{(n)}(i,j)$ for the modelled fractions obtained from the binary field I_M.

Fractions are generated for different spatial scales by changing the value of n, which can be any odd value up to $2N-1$, where N is the number of points along the longest side of the domain. A square of length $2N-1$ is the smallest that can encompass all points in the domain for squares centred at any point in the domain.

Using squares to generate the fractions is equivalent to applying the convolution kernel for a mean filter to the binary field, which is something often used in image processing (Roberts & Lean (2008)). Equation (4.4) can be rewritten as

$$O(n)(i,j) = \sum_{k=1}^{n}\sum_{l=1}^{n} I_0\Big[i+k-1-\frac{(n-1)}{2}, j+l-1-\frac{(n-1)}{2}\Big] K(n)(k,l), \quad (4.5)$$

where $K(n)(k,l)$ is the $n \times n$ kernel for a (square) mean filter. It would also be possible to use a different kernel such as a circular mean filter or Gaussian kernel, however only the square filter is used in this study.

4.2.3 Computing fractions skill scores

The mean square error (MSE) for the observed and forecast fractions for a neighbourhood of length n is given by

$$MSE_{(n)} = \frac{1}{N_x N_y} \sum_{i=1}^{n} \sum_{j=1}^{n} [O_{(n)i,j} - M_{(n)i,j}]^2. \tag{4.6}$$

By itself the MSE is highly dependent on the frequency of the event itself. A MSE skill score has been computed relative to a low-skill reference forecast (Murphy & Epstein (1989)). This is defined as the fractions skill score (FSS),

$$FSS_{(n)} = \frac{MSE_{(n)} - MSE_{(n)ref}}{MSE_{(n)perfect} - MSE_{(n)ref}} = 1 - \frac{MSE_{(n)}}{MSE_{(n)ref}}, \tag{4.7}$$

where $MSE_{(n)perf} = 0$ is the MSE of a perfect forecast for a neighbourhood length n. The reference used (MSE_{ref}) for each neighbourhood length (n) is given by

$$MSE_{(n)ref} = \frac{1}{N_x N_y} \Big[\sum_{i=1}^{N_x} \sum_{j=1}^{N_y} O^2_{(n)i,j} + M^2_{(n)i,j} \Big]. \tag{4.8}$$

This can be thought of as the largest possible MSE that can be obtained from the forecast and observed fractions.

Figure 4.2 shows the typical variation of FSS with neighbourhood length n. It has a range from 0 to 1, a forecast with perfect skill has a score of 1; a score of 0 means zero skill. Skill is lowest at the grid scale, that is, when the neighbourhood is only one grid point and the fractions are binary ones or zeros. As the size of the neighbourhood is increased, skill increases until it reaches an asymptote at $n = 2N - 1$. If there is no bias, i.e. an equal number of observed and forecast pixels exceeding the threshold, the asymptotic fractions skill score (AFSS), which is the FSS at $n = 2N - 1$, has a value of 1, indicating perfect skill over the whole domain. If there is a

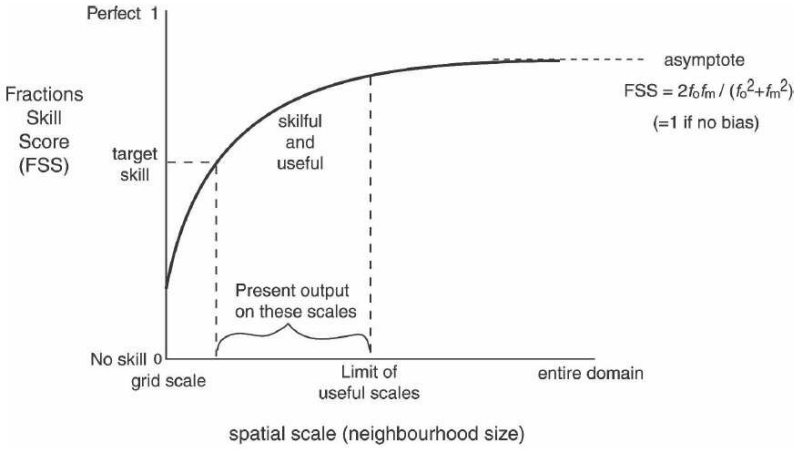

Figure 4.2: *A schematic graph of FSS against spatial scale, from Roberts & Lean (2008).*

bias then the observed frequency f_O (fraction of observed points exceeding the threshold over the domain) is not equal to the model-forecast frequency f_M, and from equations (4.6), (4.7) and (4.8) it can be shown that

$$AFSS = 1 - \frac{(f_O - f_M)^2}{f_O^2 + f_M^2} = \frac{2f_O f_M}{f_O^2 + f_M^2}, \tag{4.9}$$

which can be shown to be less than one for $f_O \neq f_M$.

Chapter 5

Statistics of model output

Two regions have been defined; a 'North' region, covering 39–50°N and 26-42°E which includes northern Turkey and the Black Sea, and a 'South' region which covers 28–39°N and 26-42°E and includes the eastern part of the Mediterranean and southern Turkey. These regions are shown in figure 5.1. Statistics described in section 4.1 have been applied to the models described in section 2.2, using the TRMM dataset as observations. The effect of applying the convolution kernel on these statistics is also investigated. FSS curves have been calculated for each region to investigate the effect of horizontal scale on model skill. These are shown here, and have been calculated for different rainfall thresholds.

5.1 Standard model skill scores

Statistical results are shown table 5.1. It can be seen that the regional model has a strong negative bias over both regions, except for summer in the south region where it has a slight positive bias. This can be seen in figure 3.2(d), where the regional model predicts some rainfall over the east coast of the Mediterranean, which is not seen in observations. In the north region HiGEM

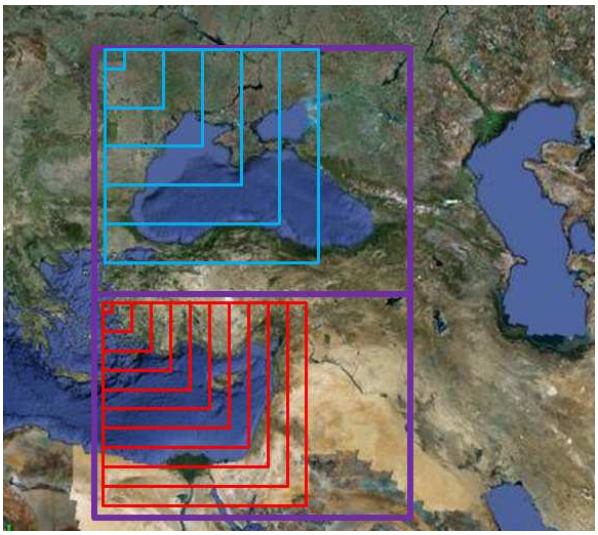

Figure 5.1: *Schematic showing the 'North' region (covering 39–50°N and 26-42°E) and the 'South' region (28–39°N and 26-42°E). Statistics for the whole of each region are discussed in section 5.1. Blue squares show the increasing spatial scales used to calculate HiGEM FSS curves, red squares show those areas used calculating RCM FSS curves (see section 5.2).*

	Bias (mm day^{-1})		RMSE (mm day^{-1}		P. Corr., ρ	
Season - Region	HiGEM	RCM	HiGEM	RCM	HiGEM	RCM
DJF - North	0.03	-0.46	1.00	0.90	0.62	0.65
JJA - North	-0.30	-0.70	0.65	0.90	0.70	0.71
DJF - South	0.32	-0.47	1.34	0.86	0.77	0.87
JJA - South	0.26	0.13	0.40	0.22	0.87	0.78

Table 5.1: *Statistical evaluation of precipitation fields over the two regions.*

displays a negative bias in summer, and a very small bias (0.03) in winter. However it is wrong to think that this indicates perfect performance in the region, when comparing plots in 3.2(a) and 3.1(e) it can be seen that HiGEM overestimates precipitation in the south of the region whilst underestimating it in the north east. These biases cancel each other out, giving a misleadingly small bias. In the south region HiGEM has positive biases in both seasons.

Root mean square error (RMSE) is somewhat dependent on the magnitude of values being compared, since when values are lower, the same relative error between model and observations would give less of an absolute error and so contribute less to the RMSE than it would had the values been higher. This is partly reflected in the lower values in summer than winter over both models for both regions, apart from the regional model in the north region, where the values of RMSE are equal. This can be explained by looking at the 2mm day^{-1} contour in the plots - in observations it encloses a large part of the domain whereas in the regional model is encloses a much smaller region. In short; the regional model shows a relatively bad performance in the north region due to a strong negative bias.

Pattern correlations for both models are similar in both regions, with both models performing better in the south region. This bodes well for the use of the models in impacts studies, since the south region contains the headwaters of the Tigris and Euphrates as well as the Fertile Crescent and the length of the Jordan - areas where accurate precipitation forecasts are

	Bias (mm day^{-1})		RMSE (mm day^{-1})		P. Corr., ρ	
Season - Region	HiGEM	RCM	HiGEM	RCM	HiGEM	RCM
DJF - North	0.03	-0.47	0.70	0.67	0.75	0.77
JJA - North	-0.29	-0.69	0.58	0.86	0.71	0.71
DJF - South	0.33	-0.46	0.81	0.67	0.91	0.93
JJA - South	0.26	0.13	0.37	0.18	0.93	0.86

Table 5.2: *Statistical evaluation of precipitation fields over the two regions after one application of the convolution kernel.*

essential for accurate predictions about the hydrology in the region.

The fields were then smoothed by applying the convolution kernel. Which is equivalent to replacing the value at each grid box by a 3 x 3 grid box centred it. The same statistics were then calculated and results are shown in table 5.2.

The first thing to notice is that all bias scores remain the same after smoothing. This is to be expected since the convolution kernel is value-preserving. The slight discrepancies (by ± 0.01) are due to some precipitation 'leaking' through the domain boundary where there is a gradient across the boundary.

RMSE values are decreased by smoothing, with a higher decrease seen for already high values; the highest reductions unanimously come in winter for both models (when precipitation is highest) and the lowest reductions in summer. This is partly because in winter RMSE values are already high and so have more error to correct and partly due to the shape of the precipitation pattern. If there is a slight offset in the predicted area of rainfall between a model and observation, then smoothing the field will give a large reduction in error. If the error however comes from a near-uniform bias, then smoothing will not significantly reduce the error.

Smoothing increases the pattern correlation for all values except for the

north region in summer. This can be at least partly attributed to the fairly uniform nature of the fields; smoothing them would not significantly change the pattern they show.

5.2 Fractions Skill Scores.

The fields were bias corrected to remove some of the effect of bias on mean square error, and fractions skill scores, described in section 4.2, were calculated for both seasons for both models. Scores were calculated for increasing spatial scales (shown in figure 5.1) for each model. These were calculated for both the north and south regions. Curves of FSS against spatial scale are shown in figures 5.2 and 5.3. Different thresholds were used in calculating the binary fields, $q \geq 0.5$, 1, 2 and 4mm day^{-1}, these correspond to (a) & (b), (c) & (d), (e) & (f) and (g) & (h) respectively for both figures 5.2 and 5.3.

It can be seen that using a lower threshold gives higher FSS scores for all spatial scales. Furthermore, using a threshold that is greater than the maximum in the field gives undefined values (since the denominator in calculating FSS, MSE_{ref}, becomes zero - see equations 4.7 and 4.8). This is observed in 5.2(h), 5.3(f) and 5.3(h), where the contour lines for the corresponding thresholds lie outside the respective domains in the precipitation fields.

For the lowest thresholds, the FSS start very close to and remain at 1. This is because the threshold is too low and has eliminated information in the field; since nearly all points will lie above the threshold, the binary fields become almost uniform 1's, which tells us nothing about the accuracy of the model.

Increasing the spatial scale through application of the convolution kernel increases the FSS skill score. This shows that the skill is lowest at the grid scale. As the scale increases the FSS asymptotes - the curve can be defined

by the rate at which it does. A curve which increases quickly at first, such as the ones in figures 5.2(g) and 5.3(b), indicates an error which can partly eliminated by looking at a slightly larger scale. This kind of curve would be expected in a case where a model predicted a precipitation field which was slightly offset from observations.

A curve such as the one in 5.3(d), which begins at zero, indicates that at the grid scale the error is the maximum it can be and none of the 1s in the binary field of the model match the 1's in the observations. The scale where the curve increases gives a measure of the skill of the model as well, the larger the scale at which it asymptotes, the bigger the difference between the model and reality.

Most curves do not asymptote to 1, as they would if they had no bias. Even though the fields have been bias corrected, this means that there is still a remnant bias in the binary fields, since the numbers of 1's in the model fields will not necessarily be equal to the number of 1's in the observed field. This effect of bias could be totally removed if percentile thresholds were used to create the binary fields, then both the model and observed fields would necessarily have the same frequency of 1's.

FSS curves have a potential usefulness in giving an objective measure to define a believable scale of prediction. If a minimum skill is defined which a predictant is required to have a greater skill than, then an FSS curve gives some idea of the sort of scale for which the model gives realistic predictions. So, looking at figure 5.2(g) for example, if a target skill were defined as $FSS \geq 0.5$, then for the regional model one would only have to look at a scale of 100km to get the required skill, whereas HiGEM output would have to be viewed on a scale of greater than 200km. Whilst looking at larger areas gives a further increase in FSS, output at these scales is less useful since information is lost - looking at too high a scale makes the time and effort put into running a high resolution model redundant.

These are just ideas of how FSS curves may be utilised; curves presented in figures 5.2 and 5.3 are largely affected by biases and the choice of thresholds - no solid conclusions can be drawn from them before these issues are resolved. The choice of target skill is something which would require further investigation also, different users of model output have different requirements and some may need much greater skill than others. The approach should be to ask what is required of the output - at what scale are predictions required. For instance, if a general trend in precipitation is needed then the FSS curve would show that a high spatial scale would give a skilful prediction. If however precipitation data on the grid scale is needed then FSS curves show that skill may be lower than is acceptable on this scale and choosing the resolution of model output to use in a study may be a trade-off between resolution and skill.

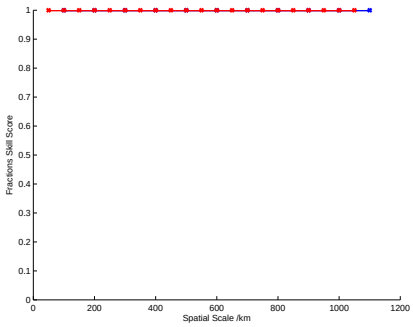

(a) 0.5 mm day $^{-1}$ threshold, DJF

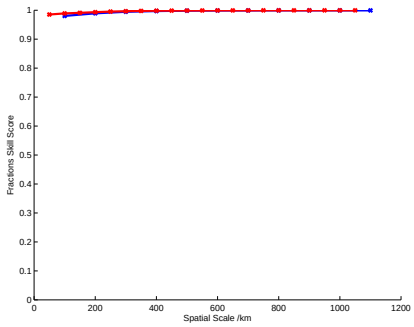

(b) 0.5 mm day $^{-1}$ threshold, JJA

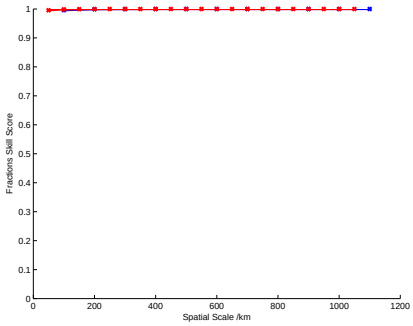

(c) 1 mm day $^{-1}$ threshold, DJF

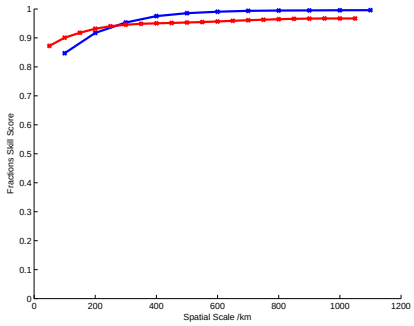

(d) 1 mm day $^{-1}$ threshold, JJA

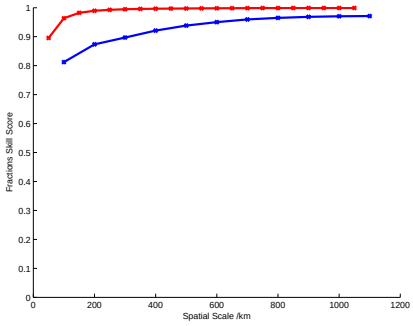

(e) 2 mm day $^{-1}$ threshold, DJF

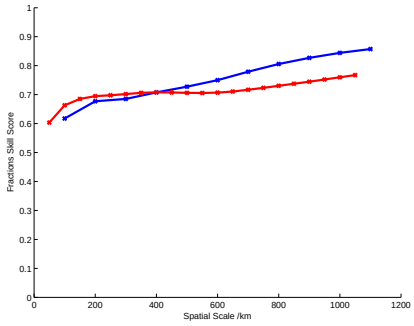

(f) 2 mm day $^{-1}$ threshold, JJA

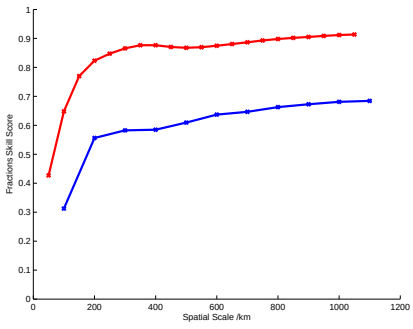

(g) 4 mm day $^{-1}$ threshold, DJF

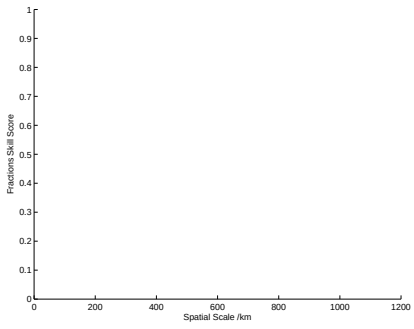

(h) 4 mm day $^{-1}$ threshold, JJA

Figure 5.2: *FSS curves for the North region. Blue curves are from HiGEM, the red curves are from the regional model.*

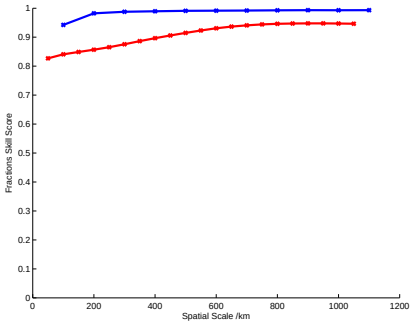

(a) 0.5 mm day $^{-1}$ threshold, DJF

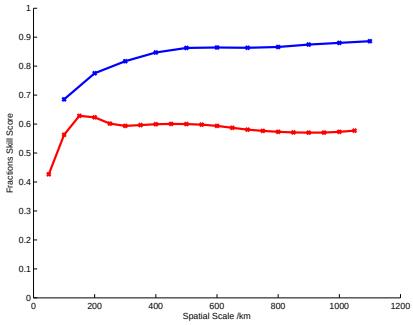

(b) 0.5 mm day $^{-1}$ threshold, JJA

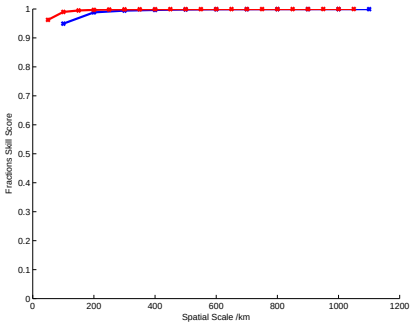

(c) 1 mm day $^{-1}$ threshold, DJF

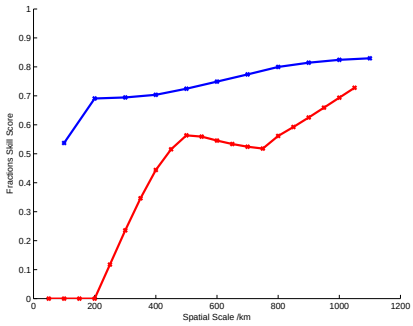

(d) 1 mm day $^{-1}$ threshold, JJA

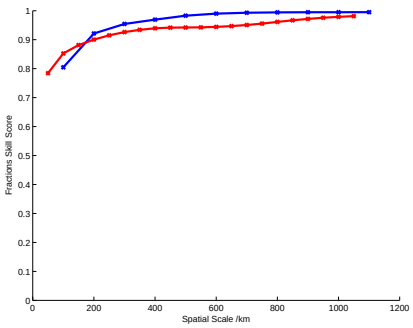

(e) 2 mm day $^{-1}$ threshold, DJF

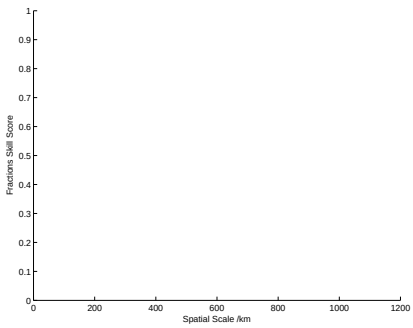

(f) 2 mm day $^{-1}$ threshold, JJA

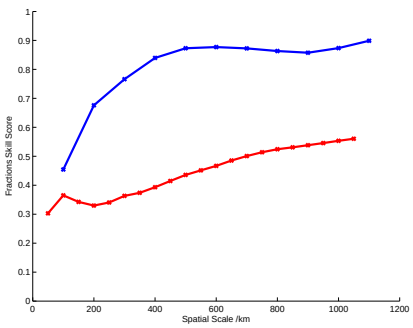

(g) 4 mm day $^{-1}$ threshold, DJF

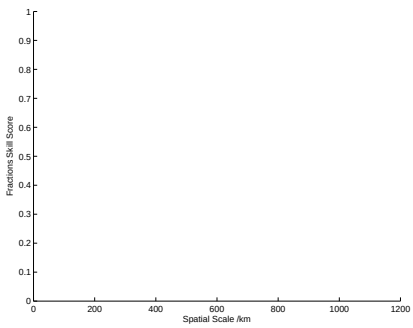

(h) 4 mm day $^{-1}$ threshold, JJA

Figure 5.3: *FSS curves for the South region. Blue curves are from HiGEM, the red curves are from the regional model.*

Chapter 6

Discussion and Conclusions

The Middle East is a semi-arid region which experiences wet winters and dry summers. Rainfall in winter comes mainly from depressions moving eastward from across the Mediterranean. In this study, two climate models, HiGEM, a 1.875° x 1.25° resolution coupled atmosphere-ocean GCM and a 0.44° x 0.44° resolution regional atmosphere-only model have been used to model the climate over the Middle East. The representation of precipitation in the models has been investigated.

Winter and summer climatologies have been compared between the two models and observations, both visually and statistically for precipitation as well other key meteorological variables. Precipitation bias, root mean square error (RMSE) and pattern correlation have been calculated for two key regions; a region encompassing the Black Sea and northern Turkey, and another encompassing southern Turkey, the Fertile Crescent and areas containing large portions of the drainage basins of the Tigris, Euphrates and Jordan.

Finally a novel method developed recently for NWP (Roberts & Lean (2008)) for examining the variation of model skill with spatial scale using thresholds has been implemented for the climatologies. Curves of fractions skill score (FSS) against horizontal scale have been plotted for both regions

using different thresholds, their shapes and what they can tell us about model performance has been discussed.

6.1 Model Evaluation

Both models represent the seasonal cycle of precipitation well, and show relatively high pattern correlations. However, HiGEM shows a slight positive bias for precipitation and the RCM shows a large negative bias. The conclusion that because the RCM has a large negative bias it is worse than HiGEM is difficult to draw however, due to error compensation. A large negative bias in the RCM could be due to an error from one problem with the model. However HiGEM could potentially have the same problem, yet have an additional problem which overestimates the precipitation; causing the biases from each problem to cancel out. It is important then to bear in mind that looking at precipitation bias alone is insufficient to draw any certain conclusions regarding model performance.

Both models underestimate the magnitude of the winds making up the Mediterranean storm track and have some problems with the region of wintertime low pressure over Cyprus. This is known as the Cyprus low and is associated with wintertime depressions moving eastwards across the Mediterranean. In HiGEM the intensity of the low is underestimated and in the RCM it is almost absent. This would have an effect on the precipitation in the Middle East; a weaker low would bring fewer weather systems to the region. The major underestimation of the Cyprus low in the RCM is likely to be a factor associated with its large negative precipitation bias.

Both models have errors in surface wind fields around the main region of precipitation around the east coast of the Mediterranean. HiGEM overestimates the convergence in the region and the RCM underestimates it. This could well be associated with the errors in precipitation amounts; ex-

tra convergence in HiGEM would give extra ascent and so give too much precipitation, and a lack of convergence in the RCM would give less ascent and so less precipitation. The RCM also has much larger errors in circulation which suggests that errors in precipitation are due to errors in model physics. However all meteorological variables are functions of each other - an error in winds leads to errors in convergence, leading to errors in precipitation. This can alter the radiation reaching the earth and so alter temperature, which in turn affects pressure patterns and therefore winds. For this reason caution should be used when attempting to attribute an error in on field to another one - all are interdependent and further study is needed to pin down the original sources of error in the models.

It has also been shown that by smoothing fields errors are reduced and pattern correlations increased. This is equivalent to viewing output on a larger scale, suggesting that future climate predictions may be made more accurate by looking at high resolution output on a lower resolution grid. This was further investigated by calculating fraction skill scores, a method novel for climate model analysis, which has been introduced recently for numerical weather prediction (Roberts & Lean (2008)).

6.2 FSS skill scores

Fractions skill scores (FSS) curves introduced recently (Roberts & Lean (2008)) have been calculated for two regions in the area, a south region containing the main band of precipitation spreading around the eastern coast of the Mediterranean, and a north region which contains the majority of the Black sea. Curves of FSS against spatial scale have been plotted, and it has been found that skill is lowest at the grid scale, asymptoting to a constant value once the scale is large enough. However output is only useful at scales which are large enough to give a high skill, but low enough not to make the

use of high resolution models pointless.

The choice of threshold in creating the binary field has been found to be important to the usefulness of the FSS curves. Too low and information is lost, the model and observation fields are mostly filled with 1's and FSS are uniformly high, regardless of spatial scale. Choosing too high a threshold is problematic also, since a model may have a low bias and so not have any values in the field above the threshold parameter, causing the FSS to be undefined. It is important therefore to choose a threshold low enough such that an acceptable number of points lie above it, yet not so low that most of the field become converted to 1's. The optimal choice of threshold is a question which requires further study, and is no doubt highly dependent on the purpose of the study.

The shape of FSS curves has been shown to give information about the usefulness of the prediction; a curve with a high initial gradient shows a field which is fairly accurate, possibly predicting the right amount and pattern of precipitation with a slight offset from the observed pattern. Thus the FSS at the grid scale is low, yet increasing the scale slightly gives a much higher skill. A curve which starts low and remains low however, either shows a prediction with poor spatial accuracy no matter what grid scale is looked at or a prediction which exhibits a large bias.

Bias has an unhelpful effect on the FSS curves by affecting the magnitude of the FSS. In this study fields were bias corrected before calculating FSS, however there is still a remnant effect in the fields - bias corrected fields for models and observations have the same average value across all grid boxes, however there will be differences in spatial variability between them. They may have different numbers of points lying above the chosen threshold, so that when binary fields are calculated model and observation fields have different numbers of 1's. Whilst the numbers of 1's are most likely closer together than they would have been had the model not been bias corrected,

they are still different, which is a cause of the bias in the FSS curves. Too much bias gives an unfairly low score and there is no easy way of standardising the effect of bias between regions, seasons and models if absolute thresholds are used. This is a major drawback of the method used in this study for caluating the FSS curves.

6.3 Future Work

A potential source of extension to this study would be using percentile thresholds to calculate binary fields for the FSS curves. Using, for example, the 95% threshold used to convert fields to binary values would automatically remove the effect of any bias since both the model and observation fields would have exactly the same number of points laying above the threshold. This would allow calculation of standardised FSS curves, making comparison between more objective.

Further statistical analysis of model output is needed before any definitive conclusions regarding the abilities of the two models can be made. It may be a useful exercise to investigate monthly indicators of precipitation. This has been used elsewhere (Evans (2004)) to test the extent to which storm track location, topography and atmospheric stability explain the modelled precipitation. In comparing any results from this analysis to results from observations, it could be shown which particular precipitation process are represented well in the models and which are not.

It is difficult to attribute performance, good or bad, to any particular feature of the two models in this study. Because only two models have been studied and they differ in both resolution and in the components they contain (i.e. one has an interactive ocean) it is hard to say with confidence that any differences in skill in an area are due to a specific component of the model. A way to make more specific conclusions about the effect of an ocean would

be to test two models at the same resolution with different components. For instance HiGEM could be evaluated against HiGAM, a model which operates at the same resolution as HiGEM but does not contain an ocean. The effect of resolution on model output could also be tested, for instance if the RCM were run at the lower HiGEM resolution as well the higher resolution.

In this study only multi year climatologies have been compared. Whilst this is a vital part of model performance, it is not the only part. Temporal variability is an aspect of the climate which has not been addressed and would be a mistake to think that good performance in spatial dimensions alone is enough for a model. A model could perform perfectly in predicting the location and magnitude of yearly averages of precipitation, however if it fails to capture temporal variability then it certainly has problems. Thus, more testing of these models should focus on the representation of temporal variability.

Another aspect of the climate which the models should be tested for is representation of extremes. In a region which has already been shown to be at risk from climate change, it is important to be able to predict with accuracy not just how much average amounts of rainfall will change, but how much the frequency of extremes will change, i.e. how often droughts and floods will occur compared to the past. One possible method of analysing extremes would be to look at quantiles; dividing model and observational data into subsets and comparing the highest and lowest sets.

The climate is intrinsically linked to the existence of human civilization and climate change is one of the biggest threats we currently face as a species. Climate models are our best chance at knowing what we can expect from the future. They can make predictions with varying levels of certainty and the drive towards better representation of climate will only improve these predictions. By validating our models in ways similar to those outlined in this study we can reduce the uncertainty of our future predictions, especially

on local scales, and with this improved knowledge we can plan for the future and we stand a better chance of overcoming the challenges we face.

References

Alpert, P., Krichak, S., Shafir, H., Haim, D. & Osetinsky, I. (2008), 'Climatic trends to extremes employing regional modeling and stastical interpretation over the eastern mediterranean', *Global Planetary Change* **63**.

Alpert, P., Stein, U. & Tsidulko, M. (2005), 'Role of sea fluxes and topography in eastern mediterranean cyclogenesis', *The Global atmosphere and ocean system* **3**(1), 55–79.

Bengtsson, L. & Hodges, K. (2006), 'Storm tracks and climate change', *Journal of Climate* **19**, 3518–3543.

Black, E. (2009), 'The impact of climate change on daily precipitation statistics in the middle east', *Submitted to Atmospheric Science Letters* .

Broccoli, A. & Manabe, S. (1992), 'The effects of orography on midlatitude northern hemisphere climates', *Journal of Atmospheric Science* **5**, 1181–1201.

Brown, O. & Crawford, A. (2009), 'Rising temperatures, rising tensions: Climate change and the risk of violent conflict in the middle east', *International Institute for Sustainable Development* .

Catto, J., Shaffrey, L. & Hodges, K. (2009), Can climate models capture the structure of extratropical cyclones? University of Reading.

Christensen, J., Hewitson, B., Busuioc, A., Chen, A., Gao, X., Held, R., Jones, R., Kolli, R., Kwon, W., Laprise, R., Magana Rueda, V., Mearns, L., Menendez, C., Raisanen, J., Rinke, A., Sarr, A., Whetton, P., Arritt, R., Benestad, R., Beniston, M., Bromwich, D., Caya, D., Comiso, J., de Elia, R. & Dethloff, K. (2007), *Climate Change 2007: The Physical Science Basis. Contribution of Working Group I to the Fourth Assessment Report of the IPCC; Chapter: Regional Climate Projections*, Cambridge University Press.

Cruz, R., Harasawa, H., Lal, M. & Wu, S. (2007), *Climate Change 2007: Impacts, Adaptation and Vulnerability. Contribution of Working Group II to the Fourth Assessment Report of the Intergovernmental Panel on Climate Change, Chapter 10: Asia*, Cambridge University Press, Cambridge, UK.

Cullen, H., Kaplan, A., Arkin, P. & Demenocal, P. (2002), 'Impact of the north atlantic oscillation on middle eastern climate and streamflow', *Climatic Change* **55**, 315–338.

Done, J., Davis, C. & Weisman, M. (n.d.), 'The next generation of nwp: Explicit forecasts of convection using the weather research and forecasting (wrf) model', *Atmospheric Science Letters* **5**, 110–117.

Earth System Research Laboratory (2009), 'Gpcc global precipitation climatology centre'. `http://www.cdc.noaa.gov/data/gridded/data.gpcc.html`.

Evans, J. (2004), 'Middle east climate simulation and dominant precipitation processes', *Int. J. of Climatology* **24**, 1671–1694.

Evans, J. (2008), '21st century climate change in the middle east', *Climatic Change* **92**, 417–432.

Evans, J. (2009), 'Global warming impact on the dominant precipitation processes in the middle east', *Theoretical and Applied Climatology, in press.* .

GoogleEarth (2009). `http://www.earth.google.co.uk/`.

Halpert, M. & Ropelewski, C. (1992), 'Surface temperature patterns associated with the southern oscillation', *Journal of Climate* **5**, 577–593.

Huffman, G.J. and Adler, R.L. and Bolvin, D.T. and Gu, G. and Nelkin, E.J. and Bowman, K.P. and Hong, Y. and Stocker, E.F. and Wolff, D.B. (2007), 'The trmm multi-satellite precipitation analysis: Quasi-global, multi-year, combined-sensor precipitation estimates at fine scale.', *Journal of Hydrometeorology* **8**(1), 38–55.

Kitoh, A., Yatagai, A. & Alpert, P. (2008), 'First super-high-resolution model projection that the ancient 'fertile crescent' will disappear in this century', *Hydrological Research Letters* **2**, 1–4.

Klein, C. & Flohn, H. (1987), 'Contributions to the knowledge of the fluctuations of the dead sea level', *Theoretical and Applied Climatology* **38**(3), 151–156.

Lorenz, E. (1969), 'Atmospheric predictability as revealed by naturally occurring analogues', *Journal of Atmospheric Science* **26**, 636–646.

Mass, C., Ovens, D., Westrick, K. & Colle, B. (2002), 'Does increasing horizontal resolution produce more skillful forecasts?', *Bulletin of the American Meteorological Society* **83**, 407–430.

McGuffie, K. & Henderson-Seller, A. (2005), *A Climate Modelling Primer, Third Edition*, Wiley.

Milly, P., Dunne, k. & Vecchia, A. (2005), 'Global pattern of trends in streamflow and water avalilability in a changing climate', *Nature* **438**, 347–350.

Murphy, A. & Epstein, E. (1989), 'Skill scores and correlation coefficients in model verification', *Monthly Weather Review* **117**, 572–581.

NASA Goddard Space Flight Center (2009), 'Global precipitation analysis'. `http://precip.gsfc.nasa.gov/`.

Olson, D. & Dinerstein, E. (2002), 'The global 200: Priority ecoregions for global conservation', *Annals of the Missouri Botanical Garden* **89**, 199–224.

Partow, H. (2001), 'The mesopotamian marshlands: Demise of an ecosystem', *UNEP - Early Warning and Assessment Technical Report* .

Peixoto, P. (2007), *Physics of Climate*, BookSurge Publishing.

Price, C., Stone, L., Huppert, A., Rajagopalan, B. & Alpert, P. (1998), 'A possible link between El Nino and precipitation in Israel', *Geophysical Research Letters* **25**, 3963–3966.

Roberts, N. & Lean, H. (2008), 'Scale-selective verification of rainfall accumulations from high-resolution forecasts of convective events', *Monthly Weather Review* **136**, 78–97.

Rodwell, M. & Hoskins, B. (1996), 'Monsoons and the dynamics of deserts', *Quarterly Journal of the Royal Meteorological Society* **122**, 1385–1404.

Ropelewski, C. & Halpert, M. (1987), 'Global and regional scale precipitation patterns associated with the el niño/southern oscillation', *Monthly Weather Review* **22**, 1606–1626.

Shaffrey, L., Stevens, I., Norton, W., Roberts, M., Vidale, P., Harle, J., Jrrar, A., Stevens, D., Woodage, M., Demory, M., Donner, J. & Clark, D. (2009), 'Uk-higem: The new uk high resolution global environment model. model description and basic evaluation.', *J. of Climate* **22**, 1861–1896.

Sharon, D. & Kutiel, H. (1986), 'The distribution of rainfall intensity in israel, its regional and seasonal variations and its climatological evaluation', *International Journal of Climatology* **6**(3), 277–291.

Slingo, J., Bates, K., Nikiforakis, N., Piggott, M., Roberts, M., Shaffrey, L., Stevens, I., Vidale, P. & Weller, H. (2009), 'Developing the next–generation climate system models: challenges and achievements', *Philosophical Transactions of the Royal Society A* **367**, 815–831.

Smith, R., Evans, J. & Oglesby, R. (n.d.), 'Mountain precipitation and hydrology in the middle east', *Yale University and NASA Marshall Space Flight Center* .

Solomon, S., Qin, D., Manning, M., Chen, Z., Marquis, M., Averyt, K., Tignor, M. & Miller, H. (2007), *Climate Change 2007: The Physical Science Basis. Contribution of Working Group I to the Fourth Assessment Report of the Intergovernmental Panel on Climate Change*, Cambridge University Press, Cambridge, UK.

Thorpe, A. (2005), 'Climate change prediction: A challenging scientific problem', *Institute of Physics* .

Uppala, S., Kallberg, P., Simmons, A., Andrae, U., Da Costa Bechtold, V., Fiorino, M., Gibson, J., Haselere, J., Hernandez, A., Kelly, G., Li, X., Onogi, K., Saarinen, S., Sokka, N., Allan, R., Andersson, E., Arpe, K., Balmaseda, M., Beljaars, A., Van De Berg, L., Bidlot, J., Bormann, N., Caires, S., Chevallier, F., Dethof, A., Dragosavac, M., Fisher, M., Fuentes, M., Hagemann, S., Holm, E., Hoskins, B., Isaksen, L., Janssen, P., Jenne, R., Mcnally, A., Mahfouf, J., Morcrette, J., Rayner, N., Saunders, R., Simon, P., Sterl, A., Trenberth, K., Untch, A., Vasiljevic, D., Viterbo, P. & Woollen, J. (2005), 'The ERA-40 re-analysis', *Quarterly Journal of the Royal Meteorological Society* **131**(612), 2961–3012.

Wang, Y., Leung, L., McGregor, J., Lee, D.-K., Wang, W.-C., Ding, Y. & Kimura, F. (2004), 'Regional climate modeling: Progress, challenges and prospects', *Journal of the Meteorological Society of Japan* **82**(6), 1599–1628.